AGU PUBLICATIONS

JGR

Journal of Geophysical Research: Space Physics

RESEARCH ARTICLE
10.1002/2016JA023054

Key Points:
- Improved inversion routine for obtaining electron density profiles from MARSIS data
- The difference is largest at larger solar zenith angles and for higher spacecraft altitudes
- The new inversion method is used to obtain a revised dependence of the peak altitude on the solar zenith angle

Correspondence to:
F. Němec,
frantisek.nemec@gmail.com

Citation:
Němec, F., D. D. Morgan, and D. A. Gurnett (2016), On improving the accuracy of electron density profiles obtained at high altitudes by the ionospheric sounder on the Mars Express spacecraft, *J. Geophys. Res. Space Physics*, *121*, 10,117–10,129, doi:10.1002/2016JA023054.

Received 13 JUN 2016
Accepted 17 SEP 2016
Accepted article online 22 SEP 2016
Published online 8 OCT 2016

On improving the accuracy of electron density profiles obtained at high altitudes by the ionospheric sounder on the Mars Express spacecraft

F. Němec[1], D. D. Morgan[2], and D. A. Gurnett[2]

[1]Faculty of Mathematics and Physics, Charles University in Prague, Prague, Czech Republic, [2]Department of Physics and Astronomy, University of Iowa, Iowa City, Iowa, USA

Abstract We attempt to improve the standard inversion routine used to obtain electron density profiles from the data measured by the Mars Advanced Radar for Subsurface and Ionospheric Sounding (MARSIS) topside radar sounder on board the Mars Express spacecraft. Artificial ionospheric traces corresponding to how the MARSIS instrument would see model electron density profiles are constructed, and they are inverted using the standard routine. Ideally, this should result in the original electron density profiles. However, it is found that discrepancies between the original and resulting electron density profiles may be significant, in particular at larger solar zenith angles and for higher spacecraft altitudes. This is due to a gap of MARSIS time delay measurements at low-sounding frequencies, and a necessity to interpolate electron density profiles in this plasma frequency range. Although the ionospheric scale height likely increases with the altitude, the standard inversion routine uses an exponential interpolation with a constant scale height. We suggest a new inversion method, which takes into account expected shapes of ionospheric profiles in the interpolation region. We verify the performance of this method both on the model electron density profiles and on real MARSIS data. We demonstrate that it seems to perform considerably better than the standard routine, in particular for higher spacecraft altitudes. Finally, we use the new inversion method to obtain a revised dependence of the peak altitude on the solar zenith angle.

1. Introduction

The Mars Advanced Radar for Subsurface and Ionospheric Sounding (MARSIS) instrument on the Mars Express spacecraft [*Chicarro et al.*, 2004] is designed for subsurface and topside ionospheric sounding [*Picardi et al.*, 2004; *Gurnett et al.*, 2005; *Jordan et al.*, 2009]. In the ionospheric sounding mode the time delay of the radar echo from the ionosphere can be used to obtain vertical electron density profiles of the topside of ionosphere directly below the spacecraft. However, the conversion to an ionospheric density profile is complicated by the fact that one must take into account the effect of plasma dispersion. It the presence of a plasma it is well known that a radar pulse propagates at the group velocity which is given by $v_g = c\sqrt{1-(f_p/f)^2}$, where c is the speed of light, f is the radar frequency, and $f_p = 8980\sqrt{n_e}$ Hz is the electron plasma frequency, where the electron density n_e is in cm^{-3}. Note that the pulse propagation velocity is less than the speed of light by a factor that depends on $(f_p/f)^2$. Normally, this factor is small so the correction from the speed of light is small, except when f is near f_p. By measuring the time delay as a function of frequency, $\Delta t(f)$, the resulting function can be "inverted" to give the plasma frequency, or equivalently the density, as a function of altitude. Specifically, the inversion can be obtained using Abel's equation [*Budden*, 1961] which is

$$z(f_p) = \frac{2}{\pi}\int_{\alpha_0}^{\frac{\pi}{2}} c\Delta t(f_p \sin\alpha)\mathrm{d}\alpha \tag{1}$$

where $\sin\alpha = f_p(z)/f$ and $\sin\alpha_0 = f_p(z_{sc})/f_p(\max)$.

Note in the above equation that the frequency of the integration goes continuously from the local plasma frequency $f_p(z_{sc})$ at the spacecraft to the maximum plasma frequency at the base of the ionosphere $f_p(\max)$. In Mars Express data these (and other equivalent) inversion techniques have a problem, because due to signal-to-noise limitations there is usually a gap in the time delay measurements between the local plasma frequency (where a very strong electrostatic resonance occurs at f_p) and the lowest frequency at which remote

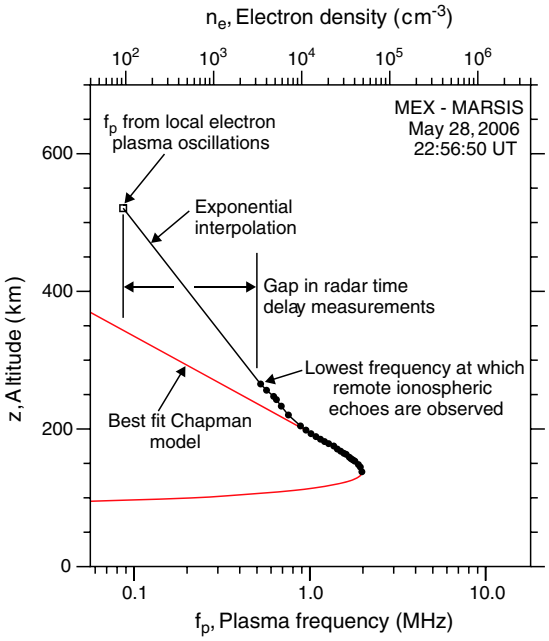

Figure 1. Example of an electron density profile obtained using the standard inversion of the MARSIS data. The lower abscissa shows the plasma frequency and the upper abscissa shows the corresponding electron density. The ordinate shows altitude. The black curve shows the electron density profile. The individual black points show the data points obtained from the ionospheric sounding. The square symbol in the upper left part of the profile shows the data point obtained from the analysis of electron plasma oscillations at the spacecraft location. No ionospheric sounding data are available in the frequency range between the local plasma frequency and about 0.55 MHz. An exponential interpolation of the density profile is used in this region, i.e., at altitudes between the highest altitude with a detectable radar sounding echo (about 275 km) and the spacecraft altitude (about 525 km). The red curve shows the best fit Chapman model of the main ionospheric layer.

echoes can be detected from the ionosphere. The situation is demonstrated in Figure 1 using the data measured on 28 May 2006 at 22:56:50 UT. The lower and upper abscissas show the plasma frequency and electron density, respectively. The individual black points show the data points obtained from the ionospheric sounding. The square symbol in the upper left part of the figure shows the data point obtained from the analysis of electron plasma oscillations at the spacecraft location. No ionospheric sounding data are available in the frequency range between the local plasma frequency and about 0.55 MHz.

In order to obtain useful results it is necessary to introduce a series of interpolated time delays between these two frequencies. So the question is, what function should be used to generate these interpolated time delays? Because the ionospheric electron density generally decreases exponentially with height, the time delay interpolation function that has been adopted by *Morgan et al.* [2008, 2013] and others is to use a logarithmic function of frequency that matches time delays at the two ends of the frequency gap. The resulting electron density profile is shown by the black curve in Figure 1. The red curve shows the best fit Chapman model of the main ionospheric layer. It can be seen that while the Chapman model gives a good fit of the experimental profile at altitudes close to the peak, it deviates considerably at higher altitudes. The observed electron densities are systematically larger than those predicted by the Chapman theory [*Gurnett et al.*, 2005, 2008], which is likely caused by a transition between the photoionization dominated Chapman-like region close to the peak and the high-altitude diffusion controlled region [*Němec et al.*, 2011]. Due to this transition, the slope of the profile (scale height) is larger at higher altitudes. The interpolation of an electron density profile using a fixed scale height value may thus be inadequate. The problem becomes particularly acute at high sounding altitudes because the frequency gap becomes larger as the plasma frequency decreases with increasing altitude.

One way to minimize the dispersion correction caused by the frequency gap in the time delay measurements is to only use radar soundings at low altitudes, i.e., near periapsis, where the frequency gap is small. For Mars Express the periapsis is lower than 400 km; i.e., it is just above the main photo-ionized Chapman layer of the ionosphere. Such low-altitude sounding gives very accurate and reliable electron density profiles, generally limited only by the accuracy of instrumental time delay and frequency measurements. However, constraining the analysis of radar sounding to such low altitudes significantly limits the amount of data available for analysis. To increase the amount of data available for analysis, we need to find an improved interpolation function that provides density profiles with good accuracy at much higher sounding altitudes, where the gap in the time delay measurements starts to produce significant errors. In this paper we seek to use the large quantity of Mars Express data available to find an improvement in the time delay interpolation function used by *Morgan et al.* [2008, 2013]. The basic approach is to use the large amount of data available (more than 10 years) to find a statistically optimum time delay function that makes inferred ionosphere density profiles

independent of altitude. This procedure essentially takes advantage of the fact that the errors introduced by the frequency gap become negligibly small at low altitudes, i.e., near periapsis.

In this paper a description of the operation of the MARSIS ionospheric sounder and the resulting data products is given in section 2. Section 3 contains a brief description of the traditionally used method by *Morgan et al.* [2013] and results of its application to model data. The improved method that we suggest and its performance on the model data is described in section 4. Section 5 presents the results obtained by applying the method to real MARSIS data. Main results are then discussed and summarized in section 6.

2. MARSIS Instrument

The MARSIS instrument does not measure directly the $\Delta t(f)$ dependence ("ionospheric trace"), but rather a wave power as a function of sounding frequency and time delay ("ionogram"). Neither the sounding frequencies nor the time delays are sampled continuously. In the normal Active Ionospheric Sounding mode of operation, there are 160 quasi-logarithmically spaced sounding frequencies between 0.1 and 5.5 MHz and 80 time delay intervals of 91.4 μs each. The ionospheric trace can be determined from an ionogram by various procedures [*Morgan et al.*, 2013], generally corresponding to the selection of a continuous $\Delta t(f)$ dependence with a large received wave intensity. Apart from the ionospheric traces, ionograms can be used to evaluate electron density [*Duru et al.*, 2008, 2011] and magnetic field magnitude [*Akalin et al.*, 2010] at the spacecraft location. An overview of principal outputs of the MARSIS instrument was given by *Gurnett et al.* [2005].

3. Standard Trace Inversion Method

The standardized routine used for the trace inversion was described by *Morgan et al.* [2013]. A problematic point concerns the shape of electron density profiles at low electron densities (high altitudes). This is due to the aforementioned gap in radar time delay measurements, when the wave power at sounding frequencies lower than $f_{\mathrm{min}} \approx 1$ MHz is typically too low for the reflected signal to be detected [*Němec et al.*, 2010]. This means that electron densities lower than about 10^4 cm^{-3} cannot be properly measured by the ionospheric sounding. In terms of the measured dependence $\Delta t(f)$, only the values of Δt at $f > f_{\mathrm{min}}$ are thus available from the sounding. In addition, the plasma frequency at the spacecraft location $f_0 = f_p(z_{\mathrm{sc}})$ (corresponding to $\Delta t = 0$) can be evaluated from the analysis of local plasma oscillations [*Gurnett et al.*, 2005; *Duru et al.*, 2008, 2011]. The only measured data relevant for the high-altitude part of the electron density profile are thus local plasma frequency f_0 and the first time delay obtained from the ionospheric sounding $\Delta t(f_1)$, where $f_1 > f_{\mathrm{min}}$. These cannot be used to unambiguously determine the electron density profile, and some further assumptions have to be made. The standard inversion routine by *Morgan et al.* [2013] assumes electron densities to exponentially decrease with altitude. As we demonstrate further, this can lead to significant inaccuracies, and it generally results in overestimating the peak altitude and electron densities.

In order to test the precision of the standard inversion routine, we apply it to $\Delta t(f)$ dependencies which correspond to model (known) electron density profiles. Theoretically, a subsequent application of the trace inversion should result back in the original electron density profiles. However, this would be the case only for continuous $\Delta t(f)$ dependencies. Considering that MARSIS samples the dependence only at predefined frequencies and discrete time delays, and, moreover, there is the aforementioned limitation at low-sounding frequencies, the obtained electron density profiles will generally differ from the original ones.

Figure 2 shows model electron densities used as a starting point of the calculation. These were calculated using the empirical model by *Němec et al.* [2011] evaluated for $F_{10.7}$ flux of 35×10^{-22} W m^{-2} Hz^{-1} and Sun-Mars distance of 1.52 AU. These values were used as they roughly correspond to average parameters relevant for Mars. However, principally the same results would be obtained for their other choice (not shown). The model electron densities are color coded in Figure 2 according to the scale at the top as a function of the altitude (ordinate) and SZA (abscissa). The white area at the bottom of the plot corresponds to altitudes below the peak. These are not accessible by the topside ionospheric radar sounding, and they were thus not included in the *Němec et al.* [2011] empirical model. The upper altitude in Figure 2 was set to 1000 km, which is close to the maximum spacecraft altitude for which reasonable sounding results may yet be obtained. The model electron densities decrease monotonically with the altitude, as expected. Moreover, while the model electron densities at low altitudes are largest at low SZAs, the situation at high altitudes is opposite. This is a result of an exponential electron density decrease assumed by the model at high altitudes, with the scale height being larger at larger SZAs. This scale height increase with SZA, clearly identifiable in local electron density data

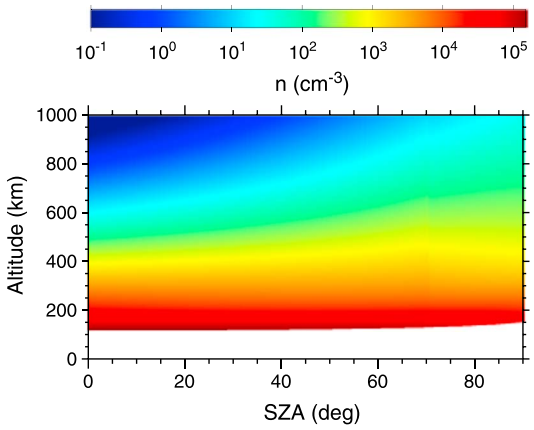

Figure 2. Model electron densities as a function of altitude (ordinate) and solar zenith angle (abscissa). Electron density values are color coded according to the color scale at the top. The white area at the bottom corresponds to the altitudes below the peak, which are not accessible by the topside ionospheric radar sounding and are not included in the model.

[*Duru et al.*, 2008; *Andrews et al.*, 2015], can be likely explained by the inclination of the magnetic field induced in the ionosphere due to the interaction with the solar wind, which impedes the vertical plasma transport [*Němec et al.*, 2011]. As the inclination of the induced magnetic field increases toward the terminator [*Brain et al.*, 2003; *Crider et al.*, 2004], the vertical plasma transport gets easier and the diffusion scale height increases.

For a given electron density profile, one can easily obtain the $\Delta t(f)$ dependence by considering the wave propagation speed in the plasma medium (dependent on the wave frequency and electron density) and numerically integrating over the path from the spacecraft altitude down to the reflection point. Having calculated the $\Delta t(f)$ dependencies, we sample them in the same way as they would be seen by the MARSIS instrument. Specifically, we replace the continuous dependence by a discrete dependence sampled at specific MARSIS sounding frequencies and time delays. Moreover, we consider that no information about the time delays Δt is available at sounding frequencies $f < f_{min}$, where $f_{min} \approx 1$ MHz. The only information available at low plasma frequencies is the plasma frequency f_0 at the spacecraft location. By applying this procedure, we obtain synthetic $\Delta t(f)$ dependencies, which correspond to a situation of "how a given electron density profile would be seen by MARSIS." Having calculated these synthetic ionospheric traces, we perform the standard inversion routine described by *Morgan et al.* [2013] to obtain electron density profiles as they would be evaluated based on the MARSIS data.

The results obtained for SZA = 60° are shown in Figure 3a. The model electron density profile (i.e., a vertical cut from Figure 2 at SZA of 60°) is shown by the black curve. This is the starting "correct" electron density profile. The lowest electron density measurable by the radar sounding is marked by the vertical dashed line. Electron density profiles obtained by inverting the corresponding synthetic MARSIS data using the standard inversion method by *Morgan et al.* [2013] are shown by the color curves. The red curve shows the electron density profile obtained assuming the spacecraft altitude of 1000 km. The blue curve shows the electron density profile obtained assuming the spacecraft altitude of 500 km. It can be seen that both profiles obtained by the inversion routine are shifted to somewhat higher altitudes/electron densities than the original profile. This shift is larger for the spacecraft altitude of 1000 km than for the spacecraft altitude of 500 km.

Figure 3b shows the ratios between the electron density profiles as they would be evaluated using the MARSIS data and real electron density profiles. Again, the red and the blue curves correspond to the spacecraft altitudes of 1000 km and 500 km, respectively. The horizontal black dashed line corresponds to one to one ratio, i.e., to the situation when the standard inversion of the synthetic MARSIS data provides exact values of electron densities. Consistent with the results from Figure 3a, the electron densities obtained by the inversion procedure are generally larger than they should be, especially at altitudes of about 300 km. The difference can be in fact rather large, with electron densities being overestimated by a factor as large as 2.3 for the spacecraft altitude of 1000 km, and by a factor as large as 1.5 for the spacecraft altitude of 500 km. We note that the density error subsequently decreases at lower altitudes (larger electron densities). This is due to larger-sounding frequencies involved, and the corresponding time delays being less affected by the—not properly determined—low-electron densities at higher altitudes.

As the results depicted in Figure 3 were obtained for a fixed value of SZA, it is instructive to investigate how the difference between the profiles obtained by the standard inversion procedure and the original profiles varies as a function of SZA. This is done in Figure 4. It shows a difference between the peak altitude evaluated using the standard inversion procedure of the MARSIS data and the real peak altitude. The used color coding is the same as in Figure 3; i.e., the red and blue points correspond to the results obtained assuming the spacecraft altitudes of 1000 km and 500 km, respectively. The results were evaluated with a 1° resolution in SZA.

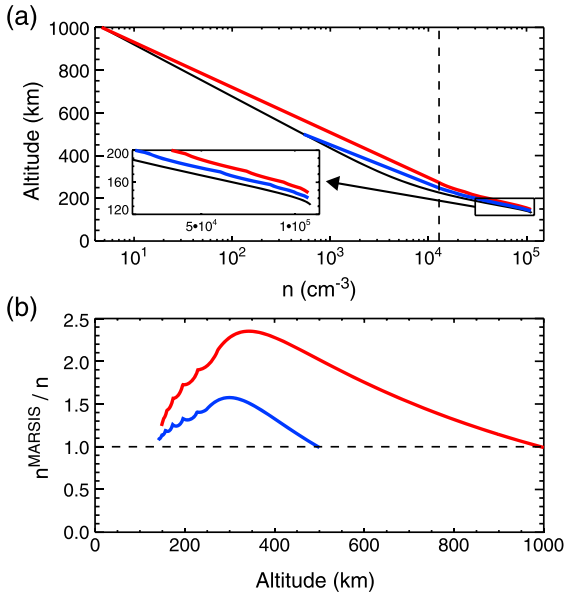

Figure 3. (a) Model electron density profile obtained for typical conditions (see text) at SZA = 60° is shown by the black curve. The blue curve shows how this electron density profile would be evaluated using the standard inversion of the MARSIS data, assuming the altitude of the Mars Express spacecraft of 500 km. The red curve shows the electron density profile obtained using the standard inversion procedure, assuming the altitude of the spacecraft of 1000 km. The vertical dashed line corresponds to the lowest electron density detectable by the radar sounding. The inset shows a zoom of the dependencies close to the peak altitude. (b) Ratio between the electron density profile as it would be evaluated using the MARSIS data assuming the spacecraft altitude of 500 km and real electron density profile is shown by the blue curve. Ratio between the electron density profile as it would be evaluated using the MARSIS data assuming the spacecraft altitude of 1000 km and the real electron density profile is shown by the red curve. The horizontal dashed line corresponds to one to one ratio.

The solid curves correspond to exponential fits of the dependencies, which were found to reasonably express the overall trends. Specifically, the red curve corresponds to $\Delta z = 1.54 \exp(0.037 \times \mathrm{SZA})$, and the blue curve corresponds to $\Delta z = 1.21 \exp(0.031 \times \mathrm{SZA})$. Note that the scatter of individual data points is due to the discreteness of the MARSIS data, in particular due to the limited resolution of the time delay Δt.

It can be seen that the peak altitudes obtained by the standard inversion are higher than the real peak altitudes. The difference is generally larger for higher spacecraft altitudes, consistent with the results from Figure 3. Moreover, the difference systematically increases with SZA. While it is within 5 km at SZAs lower than 30°, at large SZAs it becomes considerable. Specifically, at SZA of 90° the difference is as large as about 20 km for the spacecraft altitude of 500 km, and it is as large as about 45 km for the spacecraft altitude of 1000 km.

Yet another representation of the differences between electron densities obtained from the inversion and the real electron densities is shown in Figure 5. It shows a color-coded ratio between electron densities evaluated using the standard inversion and real electron densities as a function of altitude (ordinate) and SZA (abscissa). Figure 5a was obtained for the spacecraft altitude of 500 km, and Figure 5b was obtained for the spacecraft altitude of 1000 km. Again, the electron density ratios are larger for the higher spacecraft altitude, and they systematically increase with SZA. The sudden jump in the dependencies at SZA of 70° is due to the SZA discontinuity in empirical relations used by the *Němec et al.* [2011] model at high altitudes (see Figure 2). The other sudden jumps in the dependencies, which can be particularly well seen in Figure 5b at SZAs of about 11 and 62°, are again related to the discreteness of the time delay sampling by the MARSIS instrument. The value of Δt_1, i.e., the time delay corresponding to the first sounding point, is particularly important in this regard. As it is determined by MARSIS in discrete steps, its value can suddenly jump by as much as 91.4 μs. This can result in a considerable change of electron densities in the interpolated part of the electron density profile, which subsequently affects also the time delays at higher sounding frequencies. This explanation was verified by considering continuous time delay values instead of the values discretely sampled. Then, the sudden jumps disappear and smooth variations are obtained (not shown).

4. Improved Trace Inversion Method

4.1. Description of the Method

In order to remove, or at least reduce, the aforementioned problems related to the trace inversion, we suggest a new improved inversion procedure. A principal difference between the improved trace inversion method that we suggest and the traditionally used trace inversion method described by *Morgan et al.* [2013] is the assumed shape of electron density profiles in the low-density/high-altitude part. The traditional method assumes the electron density to exponentially decrease with altitude, using the same value of scale height over all the concerned altitudinal range. On the other hand, we suggest, following the statistical results by

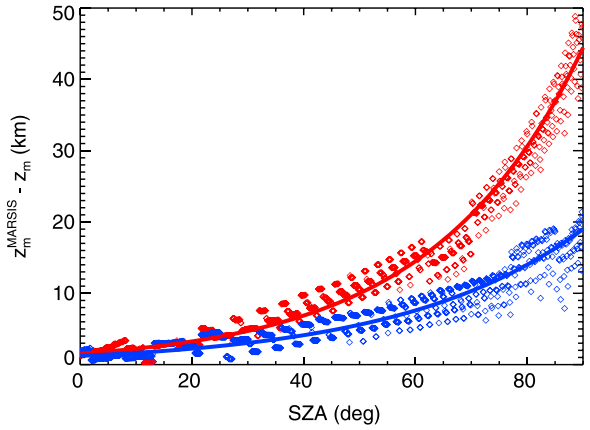

Figure 4. Difference between the peak altitude evaluated using the standard inversion of the MARSIS data and the real peak altitude. The blue points correspond to the results obtained assuming the spacecraft altitude of 500 km. The red points correspond to the results obtained assuming the spacecraft altitude of 1000 km. The solid curves correspond to exponential fits of the dependencies.

Němec et al. [2011], to allow for a smooth transition between an exponential decrease of electron densities with a given scale height at high altitudes and an exponential decrease of electron densities with another scale height at low altitudes. In other words, we allow the scale height to be larger at higher altitudes, consistent with previous MARSIS observations [*Gurnett et al.*, 2005, 2008; *Morgan et al.*, 2008].

The smooth transition between the two scale heights is achieved by using a hyperbola transition model, as described by *Watts and Bacon* [1974]. At high altitudes, electron densities are assumed to behave as $\ln n_e \propto -\theta_2 z$, where $\theta_2 = 1/H_2$ and H_2 is the appropriate scale height. Analogically, at low altitudes, electron densities are assumed to behave as $\ln n_e \propto -\theta_1 z$, where $\theta_1 = 1/H_1$. The shape of the smooth transition between the two asymptotic dependencies is characterized by the altitude z_0 where the two asymptotic dependencies intersect and by the radius of curvature which is proportional to a quantity δ. The hyperbola transition between the two dependencies can then be written as [*Watts and Bacon*, 1974]:

$$\ln n_e = C + \frac{\theta_1 + \theta_2}{2}(z - z_0) + \frac{\theta_2 - \theta_1}{2}\sqrt{(z - z_0)^2 + \frac{\delta^2}{4}} \tag{2}$$

where C is a constant. In practice, this smooth transition formula contains more variables than can be unambiguously determined from the data. For this reason, we assume that the asymptotic scale height at high altitudes $H_2 = 1/\theta_2$ corresponds to the mean scale height in the diffusion region at a given SZA according to the *Němec et al.* [2011] model:

$$H_2 = 781\text{km} \times \sin \arctan \frac{3}{40 - 0.3\ \text{SZA}} \tag{3}$$

The choice of the parameters z_0 and δ describing the transition region is somewhat arbitrary. However, once these are set, the only remaining free parameters are the asymptotic slope θ_1 at low altitudes and the constant

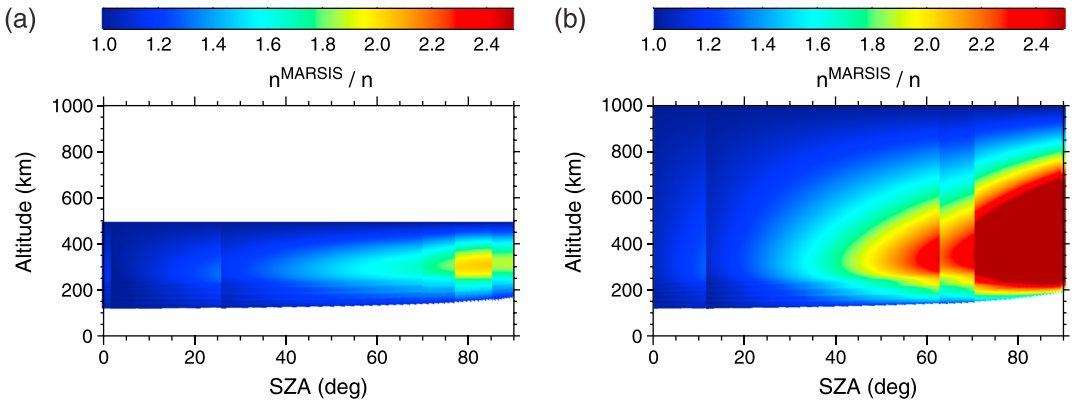

Figure 5. Ratio between electron densities evaluated using the standard inversion of the MARSIS data and real electron densities as a function of altitude (ordinate) and solar zenith angle (abscissa). The ratios are color coded according to the color scale at the top. (a) Results obtained assuming the spacecraft altitude of 500 km. (b) Results obtained assuming the spacecraft altitude of 1000 km.

C from equation (2). These are determined using the electron density at the spacecraft location n_0 and the time delay Δt_1 corresponding to the first data point from the ionospheric sounding. For a given slope θ_1, the value of C is unambiguously defined by equation (2) and a requirement of $n_e(z_{sc}) = n_0$, where n_0 is the electron density at the spacecraft location determined from the analysis of plasma oscillations. Equation (2) then provides us with the electron density profile at all altitudes between the spacecraft altitude and the altitude corresponding to the first data point from the ionospheric sounding. The appropriate time delay corresponding to this assumed electron density profile can be calculated. Then, we compare this calculated time delay with the actually measured time delay Δt_1, and we require them to be the same. If they are not, we need to modify the choice of θ_1 accordingly. Ultimately, θ_1 for which the measured time delay Δt_1 corresponds to the time delay calculated for the assumed hyperbola transition profile is found. Note that using a simple bisection method, the desired value of θ_1 can be determined with a sufficient precision in a few steps. The inversion of the trace at frequencies larger than f_1 is then done in the same way as in *Morgan et al.* [2013], i.e., the difference in the calculation is limited only to the region of high altitudes with no data points from the ionospheric sounding available. Note, however, that as the calculation of the electron density profile at lower altitudes depends on the electron density profile at higher altitudes, this difference effectively affects the entire calculated profile.

There is, however, one additional complication that we need to deal with. As the slope θ_2 at high altitudes is—for a given SZA—a fixed value, one may encounter a situation of this slope not being sufficiently steep to obtain the measured time delay Δt_1. In other words, under some circumstances, no θ_2 resulting in the observed Δt_1 exists. This generally happens for extremely large values of the electron density at the spacecraft location n_0, which would require a steeper slope θ_2 than the one assumed to work properly. In such cases, the inversion procedure that we suggest cannot be effectively used. However, one might argue that these extremely large values of n_0 are likely due to large variations of electron densities at the spacecraft altitude [*Gurnett et al.*, 2010], which, by chance, resulted in an extremely large value of n_0. It is thus questionable whether to force the algorithm in this cases to exactly fit the locally measured electron density. Instead, it might be desirable to use statistical information about electron densities expected at a given altitude and SZA [*Zhang et al.*, 2015]. We suggest to use a compromise between the two approaches. Specifically, we will assume that the plasma frequency at the spacecraft altitude is equal to the arithmetic average of the plasma frequency measured at the spacecraft location and the long-term average plasma frequency calculated using the *Němec et al.* [2011] model. Moreover, we change the value of the slope θ_2 to correspond to the slope at high altitudes obtained by the standard inversion. This decreases the values of n_0 and increases the slope θ_2 in the aforementioned extreme cases, and it seems to ensure a reasonable performance of the suggested inversion procedure even for these unusual ionospheric traces (less than 20% of the analyzed events).

As for the choice of z_0 and δ, we note that the best agreement between the shapes of the obtained profiles and those predicted by the empirical model of *Němec et al.* [2011] should not be the main criterion. The reason is that this model is based on the MARSIS data, and it thus also suffers from the aforementioned inversion-related problems, in particular in the transition region. We, can, however, use an additional desired property of the inverted data to determine the optimum values of these parameters. Specifically, the peak altitude obtained by the inversion should be independent of the spacecraft altitude. Assuming that z_0 and δ are constant, we can then determine their values using an analysis of a large amount of real inverted traces. We used the same 30,283 ionospheric traces as used previously by *Němec et al.* [2011], and we applied the new inversion routine with various choices of z_0 and δ. Then, we looked for such a choice of these parameters for which the absolute value of the correlation between the peak altitudes and the spacecraft altitudes was minimal. As the relationship is hardly linear, Spearman rank correlation coefficient [*Sheskin*, 2011] was used. Moreover, as the peak altitudes are known to depend on SZA and Sun-Mars distance [*Němec et al.*, 2011], we employed the partial rank correlation to exclude these effects. The partial rank correlation obtained for the peak altitudes determined using the standard inversion procedure was equal to 0.286. When the new inversion routine is employed, the partial rank correlation gets principally equal to zero for several possible combinations of z_0 and δ, varying from $z_0 = 250$ km and $\delta = 10$ km to $z_0 = 275$ km and $\delta = 55$ km. The exact choice of the parameters z_0 and δ then remains somewhat arbitrary. However, it has little influence on the final results. We adopted the values of $z_0 = 275$ km and $\delta = 55$ km, in order not to get too sharp change of the profile slope in the transition region.

A qualitative difference between the standard inversion method by *Morgan et al.* [2013] and the inversion method that we suggest can be seen in Figure 3a. The exponential dependence assumed by the traditional

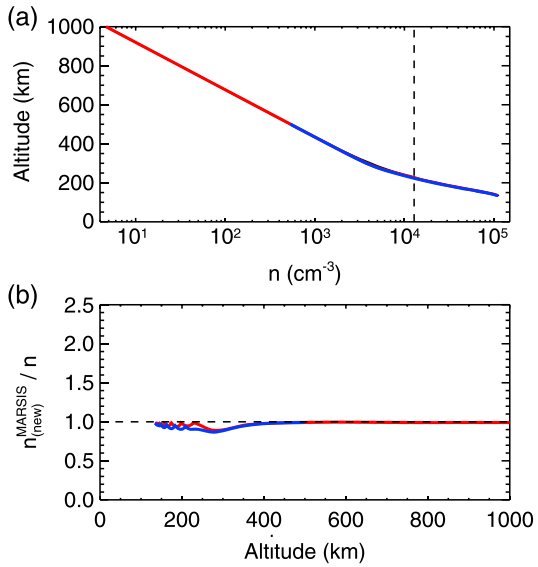

Figure 6. The same as Figure 3 but using the improved inversion procedure.

method at high altitudes has in the logarithmical plot a form of a straight line (shown in red). On the other hand, the hyperbola transition curve that we suggest to use is principally indistinguishable from the black curve shown in Figure 3a. It smoothly transits between the two slopes, corresponding to a transition from the high-altitude diffusion region to the low-altitude region controlled by photoionization. It is noteworthy that the scale height at higher altitudes is generally larger than the scale height at lower altitudes. This is the reason why the inversion method by *Morgan et al.* [2013] generally overestimates the electron densities, and, consequently, also the peak altitude. As the electron density dependence in the high-altitude region assumed in the newly suggested inversion procedure corresponds much better to the expected electron density variation, this overestimation effect principally disappears.

4.2. Application of the Method

Figure 6 is analogical to Figure 3, but the improved inversion method was used in place of the standard one. It can be seen that the differences between the electron densities obtained from the inversion and the real ones are substantially reduced, nearly nonexistent. This is the case for both low and high spacecraft altitudes. One can identify a small difference at altitudes of about 300 km, i.e., just in the transition region. However, this is possibly due to the *Němec et al.* [2011] model being imprecise in this altitudinal range due to the aforementioned problems. The performance of the improved inversion procedure at SZAs other than 60° is analyzed in Figure 7. The same format as in Figure 4 is used. Although the scatter of the data points increases with SZA, and some systematic trends may be identified (first increase, then decrease), the performance of the method is much better than the performance of the standard inversion. The difference of the peak altitudes is within about 10 km, and at SZAs lower than 80° within about 5 km. Moreover, there is principally no difference between the results obtained for low and high spacecraft altitudes.

Figure 8 uses the same format as Figure 5 to demonstrate the variation of the electron densities obtained by the improved inversion procedure with SZA. There is a systematic trend of the calculated density ratios observable at altitudes of about 300 km. Specifically, the electron densities in the transition region are lower than the model electron densities, in agreement with the results from Figure 6. However, the differences are rather small, typically within about 20%. Note that the color scale used in Figure 8 is different (zoomed) than the color scale used in Figure 5; i.e., the ratio between the electron densities obtained from the inversion and the model electron densities is generally much closer to one, as is desirable.

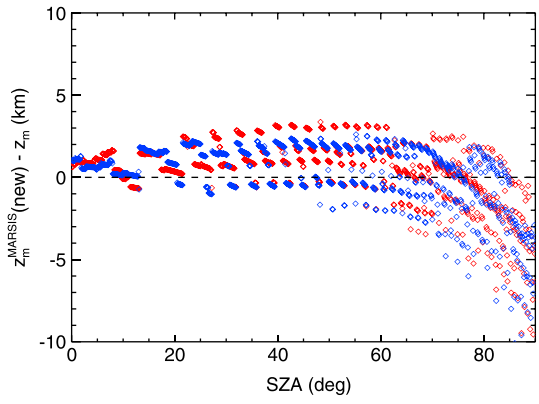

Figure 7. The same as Figure 4 but using the improved inversion procedure.

5. Application to Real MARSIS Data

Having demonstrated the performance of the improved inversion method on synthetic ionospheric traces corresponding to *Němec et al.* [2011] model electron density profiles, it is of interest to investigate its performance on real $\Delta t(f)$ dependencies measured by the MARSIS instrument. This is done in Figure 9. It shows the peak altitudes obtained using the inversion of 30,283 MARSIS traces used by *Němec et al.* [2011] as a function of SZA. Different colors of the data points correspond to different spacecraft altitudes. The blue points

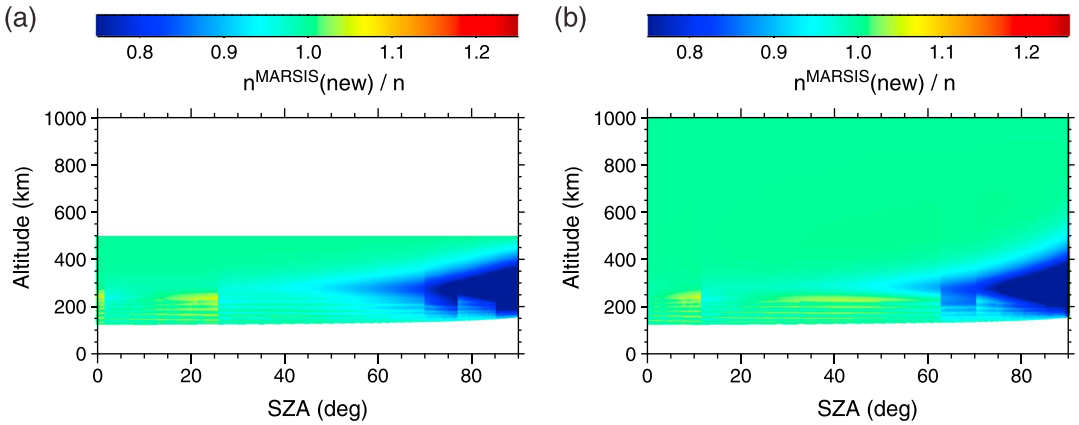

Figure 8. The same as Figure 5 but using the improved inversion procedure.

were obtained for spacecraft altitudes lower than 400 km, the green points were obtained for spacecraft altitudes between 400 and 600 km, the red points were obtained for spacecraft altitudes between 600 and 800 km, and the black points were obtained for spacecraft altitudes higher than 800 km. The short horizontal lines correspond to median values calculated in 5°-wide SZA intervals, following the same color coding. The results obtained using the standard inversion procedure and the improved inversion procedure are shown in Figures 9a and 9b, respectively. It can be seen that the peak altitudes obtained using the standard inversion procedure increase with SZA significantly faster than the peak altitudes obtained using the improved inversion procedure. In order to demonstrate that the improved inversion procedure really performs better, we investigate the behavior of the dependencies obtained for different spacecraft altitudes. As electron density profiles should be independent of the spacecraft altitude, the SZA dependencies coded by individual colors should be the same. This is roughly the case for the improved inversion procedure in Figure 9b. On the other hand, the peak altitudes obtained by the standard inversion procedure at SZAs larger than 30° are clearly larger for higher spacecraft altitudes. This is consistent with the aforementioned finding that the standard inversion method generally overestimates peak altitudes, in particular at large SZAs and for higher spacecraft altitudes. We note, however, that a weak trend in the data obtained at high spacecraft altitudes remains even when the improved inversion routine is applied. This is likely a consequence of the assumed fixed asymptotic scale height at high altitudes, which may be inadequate in some cases. Nevertheless, both visual comparison of Figures 9a and 9b, and quantitative comparison of partial rank correlations (0.286 versus principally zero) clearly show that the improved inversion routine performs much better than the traditional one.

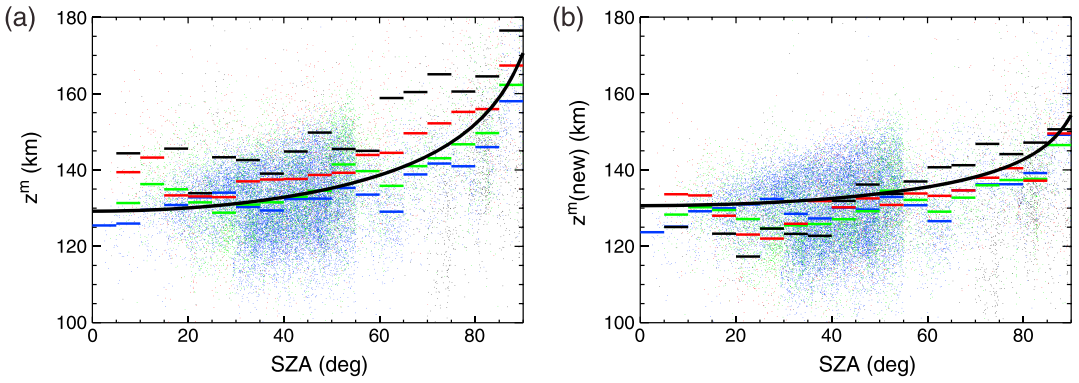

Figure 9. Peak electron densities obtained using the inversion of real MARSIS data as a function of solar zenith angle. Blue points were obtained for spacecraft altitudes lower than 400 km, green points were obtained for spacecraft altitudes between 400 and 600 km, red points were obtained for spacecraft altitudes between 600 and 800 km, and black points were obtained for spacecraft altitudes higher than 800 km. The short horizontal lines correspond to median values calculated in 5°-wide solar zenith angle intervals. The thick black curve corresponds to the best fit Chapman dependence (with z_0 and H being free parameters). (a) Results obtained using the standard inversion procedure. (b) Results obtained using the improved inversion procedure.

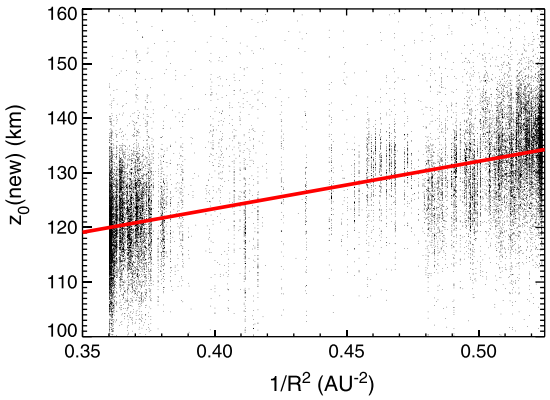

Figure 10. Altitude of peak electron density at the subsolar point as a function of $1/R^2$, where R is the Sun-Mars distance in AU. The solid red line corresponds to the best linear fit.

The thick black curves in Figures 9a and 9b correspond to the best fit Chapman dependencies, with z_0 and H being free parameters. The resulting fit parameters for the data points obtained by the standard inversion procedure are $z_0 = 129.3$ km and $H = 13.8$ km. The resulting parameters for the data points obtained by the improved inversion procedure are $z_0 = 127.0$ km and $H = 7.9$ km. The difference between the results obtained by the standard and improved inversion methods is thus considerable. Note that using the standard trace inversion routine and more stringent criteria for the selection of ionospheric traces [*Němec et al.*, 2016] would decrease the number of used traces to 26,909 and result in $z_0 = 130.2$ km and $H = 9.9$ km. The fit coefficients obtained by *Němec et al.* [2011] were $z_0 = 124.7$ km and $H = 12.16$ km. Note, however, that although they used the standard inversion method to obtain electron density profiles, they did not fit directly the obtained peak altitudes, but rather the peak altitudes corresponding to Chapman fits of individual electron density profiles. The fitting of the Chapman profiles to the electron density profiles obtained by the inversion can effectively slightly "prolong" the profile to larger electron densities and lower altitudes. Note that this tends to correct the effect of the discrete sampling of the sounding frequencies f, which necessarily leads to missing the very ends of the ionospheric traces corresponding to the highest electron densities and lowest altitudes.

We further follow the approach used by *Němec et al.* [2011] for analyzing the peak altitude dependence on the Sun-Mars distance, but we use the values of z_0 obtained using the improved inversion procedure. The obtained results are shown in Figure 10. It shows the calculated altitudes of peak electron density in the subsolar point as a function of $1/R^2$, where R is the Sun-Mars distance in AU. The red line corresponds to the best linear fit. Qualitatively, the results are principally the same as those obtained by *Němec et al.* [2011]; i.e., the peak altitudes are higher for lower Sun-Mars distances. However, the exact values of the fit coefficients are slightly different. The best fit equation is $z_0 = a/R^2 + b$ with the coefficients $a = 88.8$ km AU^2 and $b = 86.7$ km.

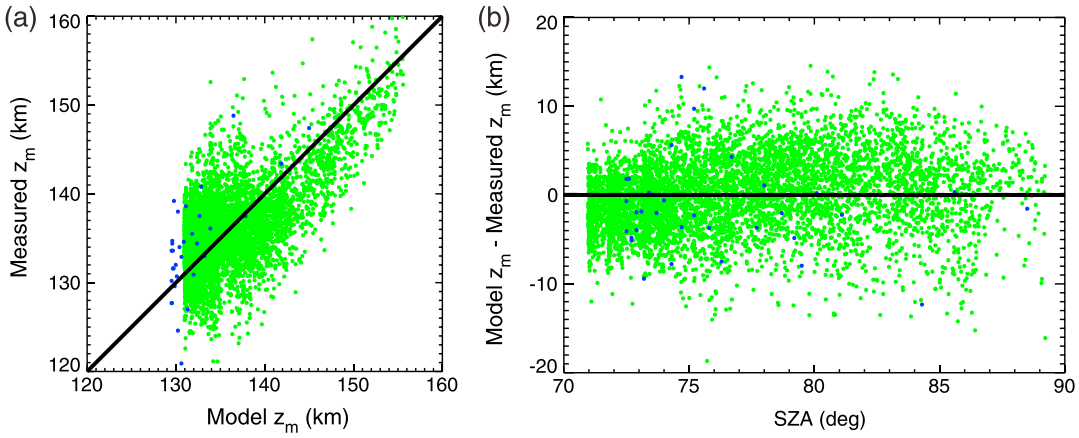

Figure 11. (a) Peak altitudes from *Kliore et al.* [1973] (blue points) and 5600 MGS RS profiles [*Hinson*, 2008] (green points) versus peak altitudes calculated using the fits to MARSIS data obtained using the improved inversion procedure. The solid black line shows the 1:1 dependence. (b) Difference between the peak altitudes determined using the fits to MARSIS data obtained using the improved inversion procedure and radio occultation measurements as a function of solar zenith angle. The same color coding as in Figure 11a is used. The horizontal black solid line shows the 1:1 dependence. The horizontal black dashed line shows the average difference of the peak altitudes (about 3.8 km).

In order to further verify the correctness of the performed inversion procedure and the peak altitude fits from Figures 9 and 10, we compare the results of this fitting ("model" parameterized by SZA and *R*) with peak altitudes determined independently from radio occultation measurements. Altogether, 36 radio occultation measurements from *Kliore et al.* [1973] and 5600 Mars Global Surveyor (MGS) radio occultation profiles [*Hinson*, 2008] were used. The results of the comparison with the MARSIS data set are shown in Figure 11. Peak altitudes from the radio occultation measurements are shown as a function of the peak altitudes calculated using the aforementioned empirical dependence based on the improved inversion procedure of the MARSIS data set in Figure 11a. The data points from *Kliore et al.* [1973] and *Hinson* [2008] data sets are shown by blue and green points, respectively. The solid black line shows the 1:1 dependence. It can be seen that although the scatter of the data points is significant, the model peak altitudes are on average in excellent agreement with the peak altitudes determined from the radio occultation measurements. This is further confirmed in Figure 11b, which shows differences between the peak altitudes evaluated from the fit and the peak altitudes from the radio occultation measurements as a function of SZA, following the same color coding as in Figure 11a. Although the SZA coverage of the radio occultation data is severely limited, only a very minor increasing trend as a function of SZA is identified. The differences of the peak altitudes are lower than 5 km in the vast majority of cases, which can be considered as good agreement.

6. Discussion and Conclusions

MARSIS measurements of the Martian ionosphere are an extremely valuable source of ionospheric data. The measured electron densities are not limited to the spacecraft location, but they, in principle, cover all altitudes down to the altitude of the peak electron density. However, some care is needed when evaluating the appropriate electron density profiles. The largest limitation of the performed radar sounding is the low radiated power at low frequencies, which prevents electron densities lower than about 10^4 cm^{-3} to be measured by the MARSIS radar sounding. Moreover, as the evaluation of the altitude where a given sounding frequency reflects relies on the time delays measured for all lower sounding frequencies (i.e., on the shape of the electron density profile at all higher altitudes), this inevitably complicates the inversion of the entire ionospheric trace.

As the experimental information is not sufficient to evaluate electron density profiles unambiguously, one needs to make additional assumptions about their shape, in particular at high altitudes. One may also limit the calculation only to ionospheric traces for which the data gap is reasonably small. This limitation, however, necessarily results in a selection bias [*Němec et al.*, 2016]. In any case, some shape of electron density profiles in the density range not covered by the ionospheric sounding needs to be assumed. The standard inversion routine by *Morgan et al.* [2013] uses a simple exponential dependence with a fixed value of the scale height over all the altitudinal region. However, the scale height of real electron density profiles is likely not constant, but it is larger in the high-altitude diffusion-controlled region than in the low-altitude region controlled primarily by the photoionization. The standard inversion routine can thus result in significant inaccuracies, in particular for large SZAs and high spacecraft altitudes. We have shown that as a result the electron densities obtained by the standard inversion routine are generally larger than they should be, and the peak altitudes are overestimated.

The trace inversion routine that we suggest attempts to remove the aforementioned problems by considering a more realistic shape of electron density profiles, using a smooth transition between two different scale heights. We have described in detail the principle of its operation. Its Interactive Data Language source code is available at http://nemec.matfyz.cz/trace_inversion. The performance of the suggested inversion routine on the model data is nearly perfect. This is clearly in part related to the routine assuming the two regions with different scale heights and a smooth transition region in between them, exactly as the *Němec et al.* [2011] model. However, several electron density profiles from radio occultation measurements show that sometimes the ionosphere is well characterized by a single topside scale height [*Withers et al.*, 2012, 2015]. In such cases the performance of the suggested inversion routine critically depends on the actual value of the topside scale height. If it is close to the average topside scale height of the *Němec et al.* [2011] model then the inversion routine works flawlessly. Should it be larger than the assumed scale height, then one may encounter a situation when the assumptions are too strong to obtain an electron density profile consistent with the measured time delay Δt_1. In such cases, the new inversion routine can be applied only with a modification which does not require the profile to exactly match the local electron density. Finally, if the assumed scale height was larger than the actual scale height of the topside ionosphere, then the new inversion routine would

provide results biased toward lower peak altitudes. Eventually, for specific synthetic electron density profiles, the results obtained by the new inversion routine may thus be worse than the results obtained by the standard inversion routine. Unfortunately, for a given ionospheric trace, there is no way to determine the actual situation in the ionosphere. Although the new inversion routine performs overall significantly better than the standard one, it might thus occasionally provide worse results, biased toward lower peak altitudes.

We further note that the asymptotic scale height at high altitudes used in the improved trace inversion is based on the same *Němec et al.* [2011] model as the testing data set; i.e., it inherently matches the testing data at high altitudes. In reality, the shape of ionospheric profiles can be significantly more complicated [*Kopf et al.*, 2008; *Withers et al.*, 2005, 2012]. Additionally, the MARSIS spacecraft may be located above the ionopause at the time of the ionospheric sounding [*Duru et al.*, 2008]. The ionopause boundary can sometimes occur at altitudes as low as about 400 km [*Han et al.*, 2014]. The assumptions of the inversion procedure would clearly not be fulfilled in such a case. However, even for the spacecraft located above the ionopause, the improved inversion procedure would — due to the steep electron density profile assumed at high altitudes — yield more realistic results than the standard inversion routine.

We have compared the performance of the standard and newly suggested inversion routines using real MARSIS data. Altogether, 30,283 ionospheric traces acquired by the MARSIS radar sounder have been used. In order to verify the correctness of the performed trace inversion, the results were divided according to the spacecraft altitude at the time of the measurement. Optimally, electron density profiles should be independent on the spacecraft altitude. However, we found, in agreement with the results obtained using the artificial testing data set, that the results obtained by the standard inversion routine exhibit a clear trend as a function of the spacecraft altitude. The newly suggested routine, on the other hand, provided results nearly independent of the spacecraft altitude. This is a clear improvement as compared to the standard routine and an indication of the correctness of the performed analysis. Finally, the results were used to obtain a revised dependence of the peak altitude on SZA, which is noticeably less steep than previously considered. The obtained peak altitudes were compared with the peak altitudes determined from the radio occultation measurements. They were found to be in a reasonable agreement. Most importantly, the overestimation of peak altitudes reported by *Němec et al.* [2011, Figure 12b] using the standard inversion procedure was removed.

The suggested trace inversion routine should be used in place of the standard one, in particular at high SZAs and for high spacecraft altitudes. Although it is computationally more expensive than the standard routine, it is still sufficiently fast to be used even on a large number of ionospheric traces, and the obtained results are more realistic and less biased.

Acknowledgments
MARSIS data are available via the ESA Planetary Science Archive (http://www.rssd.esa.int/PSA). MGS radio occultation profiles are available from the Planetary Data System (http://ppi.pds.nasa.gov/data/MGS-M-RSS-5-EDS-V1.0). The research at the University of Iowa was supported by NASA through contract 1224107 with the Jet Propulsion Laboratory.

References

Akalin, F., D. D. Morgan, D. A. Gurnett, D. L. Kirchner, D. A. Brain, R. Modolo, M. H. Acuña, and J. R. Espley (2010), Dayside induced magnetic field in the ionosphere of Mars, *Icarus*, *206*, 104–111, doi:10.1016/j.icarus.2009.03.021.

Andrews, D. J., N. J. T. Edberg, A. I. Eriksson, D. A. Gurnett, D. Morgan, F. Němec, and H. J. Opgenoorth (2015), Control of the topside Martian ionosphere by crustal magnetic fields, *J. Geophys. Res. Space Physics*, *120*, 3042–3058, doi:10.1002/2014JA020703.

Brain, D. A., F. Bagenal, M. H. Acuña, and J. E. P. Connerney (2003), Martian magnetic morphology: Contributions from the solar wind and crust, *J. Geophys. Res.*, *108*, 1424, doi:10.1029/2002JA009482.

Budden, K. G. (1961), *Radio Waves in the Ionosphere*, Cambridge Univ. Press, Cambridge, U. K.

Chicarro, A., P. Martin, and R. Trautner (2004), The Mars Express mission: An overview, in *Mars Express: The Scientific Payload*, vol. 1240, edited by A. Wilson and A. Chicarro, pp. 3–13, ESA Special Publication, Noordwijk, Netherlands.

Crider, D. H., D. A. Brain, M. H. Acuña, D. Vignes, C. Mazelle, and C. Bertucci (2004), Mars Global Surveyor observations of solar wind magnetic field draping around Mars, *Space Sci. Rev.*, *111*, 203–221.

Duru, F., D. A. Gurnett, D. D. Morgan, R. Modolo, A. F. Nagy, and D. Najib (2008), Electron densities in the upper ionosphere of Mars from the excitation of electron plasma oscillations, *J. Geophys. Res.*, *113*, A07302, doi:10.1029/2008JA013073.

Duru, F., D. A. Gurnett, D. D. Morgan, J. D. Winningham, R. A. Frahm, and A. F. Nagy (2011), Nightside ionosphere of Mars studied with local electron densities: A general overview and electron density depressions, *J. Geophys. Res.*, *116*, A10316, doi:10.1029/2011JA016835.

Gurnett, D. A., et al. (2005), Radar soundings of the ionosphere of Mars, *Science*, *310*, 1929–1933, doi:10.1126/science.1121868.

Gurnett, D. A., et al. (2008), An overview of radar soundings of the Martian ionosphere from the Mars Express spacecraft, *Adv. Space Res.*, *41*, 1335–1346.

Gurnett, D. A., D. D. Morgan, F. Duru, F. Akalin, D. Winningham, R. A. Frahm, E. Dubinin, and S. Barabash (2010), Large density fluctuations in the Martian ionosphere as observed by the Mars Express radar sounder, *Icarus*, *206*(1), 83–94, doi:10.1016/j.icarus.2009.02.019.

Han, X., et al. (2014), Discrepancy between ionopause and photoelectron boundary determined from Mars Express measurements, *Geophys. Res. Lett.*, *41*, 8221–8227, doi:10.1002/2014GL062287.

Hinson, D. P. (2008), *Mars Global Surveyor Radio Occultation Profiles of the Ionosphere — Reorganized*, vol. MGS-M-RSS-5-EDS-V1.0, NASA Planetary Data System.

Jordan, R., et al. (2009), The Mars Express MARSIS sounder instrument, *Planet. Space Sci.*, *57*, 1975–1986, doi:10.1016/j.pss.2009.09.016.

Kliore, A. J., G. Fjeldbo, B. L. Seidel, M. J. Sykes, and P. M. Woiceshyn (1973), S band radio occultation measurements of the atmosphere and topography of Mars with Mariner 9: Extended mission coverage of polar and intermediate latitudes, *J. Geophys. Res.*, *78*(20), 4331–4351, doi:10.1029/JB078i020p04331.

Kopf, A. J., D. A. Gurnett, D. D. Morgan, and D. K. Kirchner (2008), Transient layers in the topside ionosphere of Mars, *Geophys. Res. Lett.*, *35*, L17102, doi:10.1029/2008GL034948.

Morgan, D. D., D. A. Gurnett, D. L. Kirchner, J. L. Fox, E. Nielsen, and J. J. Plaut (2008), Variation of the Martian ionospheric electron density from Mars Express radar soundings, *J. Geophys. Res.*, *113*, A09303, doi:10.1029/2008JA013313.

Morgan, D. D., O. Witasse, E. Nielsen, D. A. Gurnett, F. Duru, and D. L. Kirchner (2013), The processing of electron density profiles from the Mars Express MARSIS topside sounder, *Radio Sci.*, *48*(3), 197–207, doi:10.1002/rds.20023.

Němec, F., D. D. Morgan, D. A. Gurnett, and F. Duru (2010), Nightside ionosphere of Mars: Radar soundings by the Mars Express spacecraft, *J. Geophys. Res.*, *115*, E12009, doi:10.1029/2010JE003663.

Němec, F., D. D. Morgan, D. A. Gurnett, F. Duru, and V. Truhlík (2011), Dayside ionosphere of Mars: Empirical model based on data from the MARSIS instrument, *J. Geophys. Res.*, *116*(E07003), doi:10.1029/2010JE003789.

Němec, F., D. D. Morgan, D. A. Gurnett, and D. J. Andrews (2016), Empirical model of the Martian dayside ionosphere: Effects of crustal magnetic fields and solar ionizing flux at higher altitudes, *J. Geophys. Res. Space Physics*, *121*, 1760–1771, doi:10.1002/2015JA022060.

Picardi, G., et al. (2004), MARSIS: Mars advanced radar for subsurface and ionosphere sounding, in *Mars Express: the Scientific Payload*, vol. 1240, edited by A. Wilson and A. Chicarro, pp. 51–69, ESA Special Publication, Noordwijk, Netherlands.

Sheskin, D. J. (2011), *Handbook of Parametric and Nonparametric Statistical Procedures*, 5th ed., CRC Press, Boca Raton, Fla.

Watts, D. G., and D. W. Bacon (1974), Using an hyperbola as a transition model to fit two-regime straight-line data, *Technometrics*, *16*(3), 369–373, doi:10.2307/1267666.

Withers, P., M. Mendillo, H. Rishbeth, D. P. Hinson, and J. Arkani-Hamed (2005), Ionospheric characteristics above Martian crustal magnetic anomalies, *Geophys. Res. Lett.*, *32*, L16204, doi:10.1029/2005GL023483.

Withers, P., et al. (2012), A clear view of multifaceted dayside ionosphere of Mars, *Geophys. Res. Lett.*, *39*, L18202, doi:10.1029/2012GL053193.

Withers, P., S. Weiner, and N. R. Ferreri (2015), Recovery and validation of Mars ionospheric electron density profiles from Mariner 9, *Earth Planets Space*, *67*(194), doi:10.1186/s40623-015-0364-2.

Zhang, Z., R. Orosei, Q. Huang, and J. Zhang (2015), Relationship of dayside main layer ionosphere height to local solar time on Mars and implications for solar wind interaction influence, *J. Geophys. Res. Planets*, *120*, 1427–1445, doi:10.1002/2015JE004859.